Statistical treatment of dynamical electron diffraction from growing surfaces

S. L. Dudarev
Department of Materials, University of Oxford, Parks Road, Oxford OX1 3PH, United Kingdom

D. D. Vvedensky
The Blackett Laboratory, Imperial College, Prince Consort Road, London SW7 2BZ, United Kingdom

M. J. Whelan
Department of Materials, University of Oxford, Parks Road, Oxford OX1 3PH, United Kingdom
(Received 16 May 1994; revised manuscript received 7 July 1994)

Statistical methods developed previously for the evaluation of the electrical conductivity of metals and the description of the propagation of waves through random media are applied to the problem of scattering of high-energy electrons from a rough growing surface of a crystal where the roughness is caused by local fluctuations of site occupation numbers occurring during the growth. We derive the relevant Dyson and Bethe-Salpeter equations and define the short-range order correlation functions that determine the behavior of the reflection high-energy electron diffraction (RHEED) intensities. To analyze the temporal evolution of these correlation functions, we employ an exactly solvable model of the local perfect layer growth [A. K. Myers-Beaghton and D. D. Vvedensky, J. Phys. A **22**, L467 (1989)]. Our approach makes it possible to separate individual contributions of various processes that give rise to oscillations of the RHEED reflections. We found that provided that the Bragg conditions of incidence are satisfied, it is the diffuse scattering by the disordered surface layer which is largely responsible for oscillations of the RHEED intensities. The temporal evolution of the angular distribution of the diffusely scattered electrons exhibits the effect of enhancement of the intensity of the Kikuchi lines with increasing surface disorder, as was observed experimentally [J. Zhang *et al.*, Appl. Phys. A **42**, 317 (1987)]. An explanation of the origin of this phenomenon is given using the concept of the final-state standing wave pattern.

I. INTRODUCTION

In recent years it has been recognized that reflection high-energy electron diffraction (RHEED) provides a unique tool for *in situ* monitoring of the molecular-beam epitaxial growth of surfaces of semiconductor crystals.[1,2] The observations carried out by Harris, Joyce, and Dobson[3] and Van Hove, Lent, Pukite, and Cohen,[4] and subsequent studies[5] have shown that in many cases there exists an explicit one-to-one correspondence between the number of maxima or minima on the curve describing the temporal evolution of the specular RHEED intensity and the number of new atomic layers grown on the surface of the crystal. Several theoretical models have been developed in order to understand the origin of these intensity oscillations,[6–9] and it is now a well established fact that a theoretical consideration of the problem must include multiple scattering of electrons by atoms of the crystal.[10] There exist two distinct types of scattering, namely, elastic or *coherent* scattering, which is associated with the long-range order in the distribution of atoms in the substance, and diffuse or *incoherent* scattering, resulting from local fluctuations of the parameters characterizing the structure of bulk and surface atomic layers. Both types of scattering have to be included in a consistent theoretical treatment of scattering of high-energy electrons in order to give a realistic description of the observed evolution of the diffraction pattern.

To simulate the effects of multiple coherent scattering one needs to calculate the intensities of the RHEED diffraction spots by the dynamical theory of electron diffraction. Such calculations for a surface growing during molecular-beam epitaxy have been carried out recently by Peng and Whelan[11] and Mitura *et al.*[12] The former authors employed a "systematic" approximation in calculating dynamical RHEED intensities, and only a layer coverage factor Θ_n for the nth layer was taken into account in calculating the interaction potential between the fast electron and that layer. During growth Θ_n varies between zero and unity as the arriving atomic species fill the layer and the interaction potential for the nth layer in the systematic approximation is proportional to Θ_n.[13] No statistical fluctuations of the atomic site occupation probabilities within atomic layers were considered.

At the same time there were firm experimental indications,[5,14–16] confirmed by the results of more recent studies,[17–19] that fluctuations of surface morphology and other processes leading to incoherent scattering strongly affect the temporal evolution of the RHEED pattern, and in many cases the effect of these fluctuations actually determines the entire form of the observable intensity distribution. One of the first attempts to include the effect of such fluctuations in the dynamical diffraction approach was that of Ichimiya,[9,20] who applied Kirchhoff's approximation to the description of scattering by a crystal the surface of which consisted of relatively large flat regions.[9]

Ichimiya showed that the effect of fluctuations of surface morphology can lead to a modification of the effective interaction potential between the high-energy electrons and atoms belonging to partially filled atomic layers[20] (in a more rigorous form this idea has been analysed later[21]).

An alternative formulation, which emphasizes the importance of the scattering processes by the disordered surface layer has been developed by Meyer-Ehmsen *et al.*,[22] in which a two-layer model is used to qualitatively explain the origin of the effects of diffuse scattering observed by Zhang *et al.*[23] and Larsen *et al.*[24] (see also Ref. 25). In Ref. 22 it was noted that there exist various types of incoherent scattering, some of which can be attributed to the effects of surface disorder, while others result from inelastic scattering followed by vibrational and electronic excitations in the crystal bulk (for a discussion of the effects of inelastic scattering in RHEED, see Ref. 26). A simple qualitative model which takes the surface disorder into account in terms of refraction and total reflection of waves was proposed by Lehmpfuhl *et al.*[27]

Recently, Korte and Meyer-Ehmsen[28–30] have developed an approach which is based on the first-order perturbation expansion of the nonlinear equations for the so-called R matrix. The difference between the exact and the configuration averaged potential was considered as a perturbation, giving rise to a contribution to the surface reflectivity resulting from the nonperiodic part of the interaction. This approach requires averaging bilinear combinations of the first-order terms thus obtained which, in some cases, can be performed analytically. In other cases, the problem of averaging bilinear combinations of the nonlinear R-matrix equations may encounter difficulties (e.g., when interlayer correlations have to be taken into account), in which case the application of the technique described in Refs. 28–30 would require explicit numerical computation of the intensity distributions for various statistical configurations of the system.

At present, therefore, there exists no consistent approach to describing the scattering of high-energy electrons from a growing surface which takes into account both multiple coherent and multiple incoherent scattering, and which would in principle allow us to avoid performing statistical averaging of the *numerically computed* scattering cross section over all possible configurations of the system. The stimulus for formulating such an approach is provided largely by recent progress in the understanding of the statistics of the microscopic dynamics of molecular-beam epitaxial growth[31–34] and the nonlinear kinetics of transport of atomic species on growing surfaces.[35–38] In fact, there are now available both analytical approaches (see, e.g., Ref. 34) and numerically manageable techniques,[33] which make it possible to analyze the temporal evolution of the many-particle correlation functions characterizing the nonequilibrium density fluctuations in the growing surface layer. The remaining and largely unsolved question concerns the possibility of reliably determining these correlation functions from the experimentally observed RHEED patterns.

In this paper, we develop a method which makes this problem more tractable for analytical and numerical study. Our method is based on a generalization of the techniques developed previously for the evaluation of the conductivity of metals containing randomly distributed impurities,[39] the calculation of amplitudes and phases of waves propagating through a random medium[40–43] for the case of diffraction of high-energy electrons by a statistically disordered growing surface. We formulate the Dyson equation describing multiple *coherent* scattering of electrons by the averaged distribution of atoms over the lattice sites, and the Bethe-Salpeter equation, which takes into account the processes of multiple *incoherent* scattering of the electrons by fluctuations of the interaction potential occurring in the surface layers of the crystal.

One feature of our formulation which distinguishes our method from previous approaches to the problem is the possibility of proving the statement that the system of Dyson and Bethe-Salpeter equations is self-consistent and satisfies the requirement of conservation of the total current density. The importance of this point follows from the simple observation that the total intensity of the RHEED diffraction spots in many cases does not exceed several percent of the incident beam intensity, while it is well known that the total probability of an electron being scattered towards the backward hemisphere at grazing incidence often exceeds 80%.[44] An implementation of the probability conservation principle makes it possible to classify various processes according to their contribution to the RHEED pattern and to determine which of them are responsible for the observable temporal evolution of the RHEED intensities. One of our conclusions is that, provided the Bragg conditions of incidence are satisfied, it is the diffuse (incoherent) scattering by fluctuations of the interaction potential in the disordered surface layer which gives rise to the RHEED intensity oscillations. We establish the form of the correlation functions which describe the evolution of the surface morphology in relation to the temporal behavior of the RHEED diffraction pattern. We show that in the case where the short-range disorder dominates, the diffuse scattering cross section is a functional of the two-particle *connected correlation function*[45] characterizing the distribution of pairs of atomic species among the layers of the growth front. Making use of an exactly solvable model,[35] we can evaluate this correlation function analytically, and follow the temporal evolution of the diffuse RHEED intensity distribution. We find that, provided the position of the specular reflection lies in the vicinity of a particular Kikuchi line, the intensity of this line is enhanced strongly with increasing surface disorder, as was observed by Zhang *et al.*[23].

II. THE DYSON AND THE BETHE-SALPETER EQUATIONS

As is well known the wave function of the electron is not an observable quantity and it is the bilinear combination of two wave functions which is relevant to the probability distribution and which can be employed for evaluation of the matrix elements of any quantum-mechanical operator (see, e.g., Ref. 46), for instance, the current

density of scattered electrons. In the statistical theory of scattering we are therefore interested in the determination of the function which describes the propagation of an electron from the source towards the detector through a medium, only the statistical properties of which (i.e., some average values and their momenta) are known. If $G(\mathbf{r},\mathbf{r}')$ is the Green's function which describes the propagation of an electron from the source $S(\mathbf{r}')$ towards the observation point $\mathbf{r}$ through a particular statistical configuration of a medium, then the wave function is given by

$$\Psi(\mathbf{r}) = \int d\mathbf{r}' G(\mathbf{r},\mathbf{r}') S(\mathbf{r}'), \tag{1}$$

and the quantity to be evaluated in order to calculate the scattered *intensity* is

$$\begin{aligned}\Pi(\mathbf{r},\mathbf{r}_1|\mathbf{r}',\mathbf{r}_1') &= \langle G(\mathbf{r},\mathbf{r}') G^*(\mathbf{r}_1,\mathbf{r}_1')\rangle \\ &\equiv \langle G(\mathbf{r},\mathbf{r}') G^\dagger(\mathbf{r}_1',\mathbf{r}_1)\rangle,\end{aligned} \tag{2}$$

where $\langle\cdots\rangle$ denotes an average over all the possible configurations of the system and $\hat{G}^\dagger$ is the Hermitian conjugate of $\hat{G}$. Here we are primarily interested in the case where fluctuations result from statistical disorder occurring in the distribution of atoms over the lattice sites and we do not consider dynamical fluctuations, particularly electronic excitations, methods of treating which have been developed recently.[47,48] If the wave function $\Psi(\mathbf{r})$ satisfies the Schrödinger equation

$$\left[-\frac{\hbar^2}{2m}\nabla^2 + U(\mathbf{r})\right]\Psi(\mathbf{r}) = E\Psi(\mathbf{r}), \tag{3}$$

where $E = \hbar^2 k^2/2m$, then $G(\mathbf{r},\mathbf{r}')$ can be defined as a solution of the equation

$$\left[E + \frac{\hbar^2}{2m}\nabla^2 - U(\mathbf{r})\right] G(\mathbf{r},\mathbf{r}') = \delta(\mathbf{r}-\mathbf{r}'). \tag{4}$$

Formally, the solution of (4) can be represented in the form

$$\hat{G} = \frac{1}{E - \hat{K} - \hat{U} + i0}, \tag{5}$$

where $\hat{K}$ and $\hat{U}$ denote kinetic and potential energy operators. We now consider the product $\hat{G}\hat{G}^\dagger$ and proceed to find the average of this quantity. We define the fluctuating part of the interaction by

$$\delta\hat{U} = \hat{U} - \langle\hat{U}\rangle, \tag{6}$$

and expand each of the Green's functions entering $\langle\hat{G}\hat{G}^\dagger\rangle$ in a Born power series over $\delta\hat{U}$, namely,

$$\begin{aligned}\hat{\Pi} = \langle\hat{G}\hat{G}^\dagger\rangle = \Big\langle &\Big[\frac{1}{E-\hat{K}-\langle\hat{U}\rangle+i0} + \frac{1}{E-\hat{K}-\langle\hat{U}\rangle+i0}\delta\hat{U}\frac{1}{E-\hat{K}-\langle\hat{U}\rangle+i0} \\ &+\frac{1}{E-\hat{K}-\langle\hat{U}\rangle+i0}\delta\hat{U}\frac{1}{E-\hat{K}-\langle\hat{U}\rangle+i0}\delta\hat{U}\frac{1}{E-\hat{K}-\langle\hat{U}\rangle+i0} + \cdots\Big] \\ &\times\Big[\frac{1}{E-\hat{K}-\langle\hat{U}\rangle-i0} + \frac{1}{E-\hat{K}-\langle\hat{U}\rangle-i0}\delta\hat{U}\frac{1}{E-\hat{K}-\langle\hat{U}\rangle-i0} \\ &+\frac{1}{E-\hat{K}-\langle\hat{U}\rangle-i0}\delta\hat{U}\frac{1}{E-\hat{K}-\langle\hat{U}\rangle-i0}\delta\hat{U}\frac{1}{E-\hat{K}-\langle\hat{U}\rangle-i0} + \cdots\Big]\Big\rangle,\end{aligned} \tag{7}$$

where we have taken account of the fact that both $\hat{K}$ and $\hat{U}$ are Hermitian operators.

To carry out the averaging in Eq. (7) we use the diagrammatic approach proposed by Edwards[39] and described in detail by Abrikosov, Gorkov, and Dzyaloshinskii.[40] We represent each of the Green's functions $\hat{G}$ and $\hat{G}^\dagger$ in the form of the series of diagrams as depicted in Fig. 1. The meaning of each diagram is evident from comparison of Fig. 1 with the structure of each of the two series in the right-hand side of Eq. (7). Performing step-by-step averaging of various terms resulting from multiplication of these two series, and using the rules described in Ref. 39, we arrive at the sequence of diagrams shown in Fig. 2.

There exist explicit analytical expressions corresponding to each of the diagrams shown in Fig. 2. For example, the diagram marked (f) in Fig. 2 can be represented in the analytical form as follows:

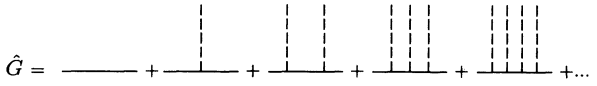

FIG. 1. The diagrammatic representation of the Green's function $\hat{G}$.

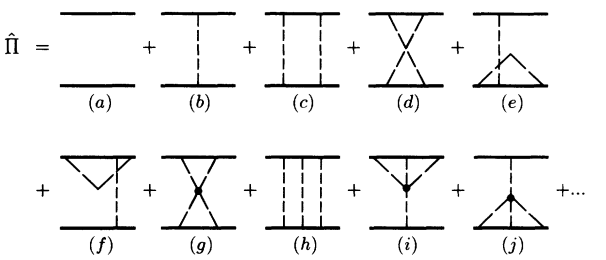

FIG. 2. The series of diagrams representing various terms resulting from averaging of the product of two Green's functions.

FIG. 3. The Bethe-Salpeter equation.

FIG. 5. The Dyson equation.

$$\frac{1}{E-\hat{K}-\langle\hat{U}\rangle+i0}\delta\hat{U}\frac{1}{E-\hat{K}-\langle\hat{U}\rangle+i0}\delta\hat{U}\frac{1}{E-\hat{K}-\langle\hat{U}\rangle+i0}\delta\hat{U}\frac{1}{E-\hat{K}-\langle\hat{U}\rangle+i0}\times\frac{1}{E-\hat{K}-\langle\hat{U}\rangle-i0}\delta\hat{U}\frac{1}{E-\hat{K}-\langle\hat{U}\rangle-i0}, \tag{8}$$

where each pair of operators $\delta\hat{U}$ connected by a dashed line corresponds to the correlation function of the form $\langle\delta\hat{U}\delta\hat{U}\rangle$ [note that in accordance with the definition (6) we have $\langle\delta\hat{U}\rangle = 0$]. Analyzing the structure of various combinations of diagrams we see that the entire infinite sequence of diagrams can be generated by iterating the equation shown in Fig. 3, where the filled rectangle represents the sequence of nonrepeating diagrams depicted in Fig. 4. The thick lines in Figs. 2, 3, and 4 correspond to the averaged Green's functions $\langle\hat{G}\rangle$ and $\langle\hat{G}^\dagger\rangle$ satisfying the equation shown in diagrammatic form in Fig. 5. In Fig. 5 the filled circle represents the series of nonrepeating diagrams depicted in Fig. 6. The diagrammatic relationships shown in Fig. 3 and Fig. 5 are the Bethe-Salpeter and Dyson equations, respectively. The basic advantage of the diagrammatic representation of these equations consists of the possibility of classification of various processes of incoherent scattering with respect to their contribution to the averaged direct product of two Green's functions $\hat{\Pi} = \langle\hat{G}\hat{G}^\dagger\rangle$.

Considering the problem of scattering of a fast electron ($\sim 10^4$–10^5 eV) by an atom, we notice that there exist two inequalities which make it possible to separate the diagrams entering the Dyson and the Bethe-Salpeter equations into two groups, with one of these groups giving the major contribution to the cross section. The first inequality follows from comparing the electron wavelength λ with the effective radius of screening $r_{\rm scr}$ of the potential of an atom.[49] For high-energy electrons

$$\lambda \ll r_{\rm scr}, \tag{9}$$

which results in the scattering cross section of electrons by atoms being strongly peaked in the forward direction, i.e., $|f(\pi)|/|f(0)| \ll 1$, where $f(\theta)$ is the amplitude of scattering.

Another inequality which often holds for fast electrons (the kinetic energy of which is in excess of 10 keV) is the condition for the validity of the Born formula, namely,

$$\hbar^2 k/r_{\rm scr} m > \langle|\delta U(\mathbf{r})|\rangle, \tag{10}$$

where $k = 2\pi/\lambda$. This justifies the acceptability of the approximation which is quadratic in $\delta\hat{U}$ and which in many cases makes it possible to obtain reliable qualitative results even beyond the limits defined by inequality (10) (see, e.g., the discussion in Refs. 40 and 21).

Application of the inequality (9) to the series of diagrams shown in Fig. 6 and Fig. 4 rules out all the diagrams containing crossing lines, which describe processes involving at least one large-angle scattering event. The second inequality (10) makes it possible to neglect all the diagrams containing more than two connected dashed lines, each of which corresponds to the fluctuating part of the interaction. As a result, the Bethe-Salpeter and Dyson equations acquire the following forms, respectively:

$$\hat{\Pi} = \langle\hat{G}\rangle\langle\hat{G}^\dagger\rangle + \langle\hat{G}\rangle\langle\delta\hat{U}\hat{\Pi}\delta\hat{U}\rangle\langle\hat{G}^\dagger\rangle\ , \tag{11}$$

and

$$\langle\hat{G}\rangle = \hat{G}_0 + \hat{G}_0\langle\delta\hat{U}\langle\hat{G}\rangle\delta\hat{U}\rangle\langle\hat{G}\rangle\ , \tag{12}$$

where $\hat{G}_0 = (E - \hat{K} - \langle\hat{U}\rangle + i0)^{-1}$. It should be noted that Eq.(12) coincides with Eq.(39.7) of Ref. 40, which was derived by making use of arguments similar to those outlined above.

Using (2), we can define the statistically averaged one-particle density matrix of the high-energy electron as

$$\rho(\mathbf{r},\mathbf{r}_1) = \int d\mathbf{r}' d\mathbf{r}_1' \Pi(\mathbf{r},\mathbf{r}_1|\mathbf{r}',\mathbf{r}_1') S(\mathbf{r}') S^*(\mathbf{r}_1'). \tag{13}$$

As follows from (11), this density matrix satisfies the

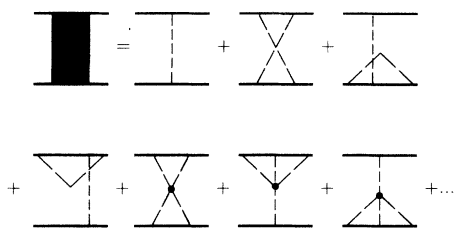

FIG. 4. The sequence of nonrepeating diagrams entering the Bethe-Salpeter equation.

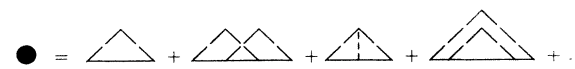

FIG. 6. The sequence of nonrepeating diagrams entering the Dyson equation.

equation

$$\hat{\rho} = \hat{\rho}_0 + \langle\hat{G}\rangle\langle\delta\hat{U}\hat{\rho}\delta\hat{U}\rangle\langle\hat{G}^\dagger\rangle, \tag{14}$$

the real space representation of which is

$$\rho(\mathbf{r},\mathbf{r}') = \rho_0(\mathbf{r},\mathbf{r}') + \int\int d\mathbf{R}d\mathbf{R}'\langle G(\mathbf{r},\mathbf{R})\rangle\langle G^*(\mathbf{r}',\mathbf{R}')\rangle \times\langle\delta U(\mathbf{R})\delta U(\mathbf{R}')\rangle\rho(\mathbf{R},\mathbf{R}'). \tag{15}$$

The first term on the right-hand side of Eq. (15) represents the incident wave and the associated elastic scattering. The second term on the right-hand side has the same meaning as the collision integral in the classical Boltzmann transport equation. In other words, the approach employing Eq. (15) can be considered as the quantum-mechanical generalization of the theory of multiple scattering, the classical counterpart of which is based on the transport equation. An important difference between the classical approach and the present quantum-mechanical consideration lies in the fact that Eq. (15) describes multiple incoherent scattering in the averaged potential field $\langle U(\mathbf{r})\rangle$, and generally speaking there exists no inequality restricting the rate of variation of this field within the effective range characterizing separate scattering events by statistical fluctuations of the interaction potential.

Before deriving approximate solutions of Eqs. (12) and (14), we first prove that these equations are self-consistent and that they conserve the total number of particles in a closed system. The quantum-mechanical current density is given by

$$\mathbf{j}(\mathbf{r}) = \frac{i\hbar}{2m}\left(\nabla' - \nabla\right)\rho(\mathbf{r},\mathbf{r}')\Big|_{\mathbf{r}=\mathbf{r}'}. \tag{16}$$

Therefore

$$\begin{aligned}\mathrm{div}\{\mathbf{j}(\mathbf{r})\} &= -\frac{i\hbar}{2m}\left(\nabla^2 - \nabla'^2\right)\rho(\mathbf{r},\mathbf{r}')\Big|_{\mathbf{r}=\mathbf{r}'} \\ &= \frac{i}{\hbar}[\hat{K}\hat{\rho}]\Big|_{\mathbf{r}=\mathbf{r}'},\end{aligned} \tag{17}$$

where $[\hat{K}\hat{\rho}] = \hat{K}\hat{\rho} - \hat{\rho}\hat{K}$ is the commutator of $\hat{K}$ and $\hat{\rho}$. The conservation of the total number of particles requires the flux of $\mathbf{j}$ to vanish over an arbitrary surface Σ with area element $d\mathbf{a}$ and volume V enclosing the crystal. This flux is given by

$$\int_\Sigma d\mathbf{a}\,\mathbf{j}(\mathbf{r}) = \int_V d\mathbf{r}\,\mathrm{div}\{\mathbf{j}(\mathbf{r})\} = \frac{i}{\hbar}\mathrm{Tr}[\hat{K}\hat{\rho}]. \tag{18}$$

Therefore we need to show that the trace of the commutator $[\hat{K}\hat{\rho}]$ vanishes. We first note that according to Eq. (12)

$$\langle\hat{G}\rangle^{-1} = \hat{G}_0^{-1} - \langle\delta\hat{U}\langle\hat{G}\rangle\delta\hat{U}\rangle. \tag{19}$$

We also have

$$\hat{G}_0^{-1} = E - \hat{K} - \langle U\rangle, \tag{20}$$

$$\hat{\rho}_0 = \langle\hat{G}\rangle\hat{S}\hat{S}^\dagger\langle\hat{G}^\dagger\rangle, \tag{21}$$

where $\hat{S}$ is the source function defined in Eq. (1), and $\langle\hat{G}\rangle^{-1} = E - \hat{K} - \hat{U}_{\mathrm{eff}}$, where $\hat{U}_{\mathrm{eff}}$ is the non-Hermitian potential defined later [Eq. (35)].

Consider the operator $\hat{Q}$ defined by

$$\hat{Q} = \langle\hat{G}\rangle^{-1}\hat{\rho} - \hat{\rho}\langle\hat{G}^\dagger\rangle^{-1}. \tag{22}$$

We evaluate $\mathrm{Tr}\hat{Q}$ by substituting from Eqs. (19) and (20) and noting that $\mathrm{Tr}\{\langle\hat{U}\rangle\hat{\rho}\} = \mathrm{Tr}\{\hat{\rho}\langle\hat{U}\rangle\}$. This leads to an expression for $\mathrm{Tr}[\hat{K}\hat{\rho}]$ in terms of $\mathrm{Tr}\hat{Q}$ and additional terms. Alternatively, $\mathrm{Tr}\hat{Q}$ can be obtained by substituting from Eq. (14) for $\hat{\rho}$, noting that from (21) both $\langle\hat{G}\rangle^{-1}\hat{\rho}_0$ and $\hat{\rho}_0\langle\hat{G}^\dagger\rangle^{-1}$ are zero, since the source function $\hat{S}$ vanishes inside Σ. We obtain

$$\begin{aligned}\mathrm{Tr}[\hat{K}\hat{\rho}] = {}& \mathrm{Tr}\{\langle\hat{G}\rangle\langle\delta\hat{U}\hat{\rho}\delta\hat{U}\rangle\} - \mathrm{Tr}\{\langle\delta\hat{U}\hat{\rho}\delta\hat{U}\rangle\langle\hat{G}^\dagger\rangle\} \\ &+\mathrm{Tr}\{\hat{\rho}\langle\delta\hat{U}\langle\hat{G}^\dagger\rangle\delta\hat{U}\rangle\} - \mathrm{Tr}\{\langle\delta\hat{U}\langle\hat{G}\rangle\delta\hat{U}\rangle\hat{\rho}\}.\end{aligned} \tag{23}$$

Since the trace remains invariant under cyclic interchange of operators and $\hat{\rho}$ and $\langle\hat{G}\rangle$ (being statistically averaged) may be moved freely through the angular averaging brackets, we arrive at the result

$$\mathrm{Tr}[\hat{K}\hat{\rho}] = 0, \tag{24}$$

which leads to the conservation of the total number of particles. In what follows we use this condition for the quantitative evaluation of individual contributions to the cross section resulting from various processes of incoherent scattering and for identifying the dominant mechanism behind the temporal evolution of the RHEED intensities.

III. THE LOCAL PERFECT LAYER GROWTH MODEL

As follows from Eqs. (11) and (12), or (15), within the approximation which is quadratic in $\delta\hat{U}$, it is the correlator $\langle\delta U(\mathbf{r})\delta U(\mathbf{r}')\rangle$ which is responsible for the contribution of (multiple) incoherent scattering to the RHEED pattern. Representing the interaction potential in the form of a sum of potentials of separate atoms

$$U(\mathbf{r}) = \sum_a n_a U(\mathbf{r} - \mathbf{R}_a), \tag{25}$$

where the summation is performed over *all* the sites of the infinite three-dimensional lattice of the crystal, and n_a is the occupation number of a particular site, we arrive at

$$\langle\delta U(\mathbf{r})\delta U(\mathbf{r}')\rangle = \sum_{a,b} U(\mathbf{r} - \mathbf{R}_a)U(\mathbf{r}' - \mathbf{R}_b) \times(\langle n_a n_b\rangle - \langle n_a\rangle\langle n_b\rangle). \tag{26}$$

The averaged occupation number $\langle n_a\rangle$ in this equation represents the probability Θ_a of finding an atom at the lattice site a, which in the case of a growing surface has the same meaning as the coverage of the layer containing the site a. The quantity $\nu_{ab} = \langle n_a n_b\rangle$ denotes the probability of finding both atomic sites a and b occupied. The function $F_{ab} = \nu_{ab} - \Theta_a\Theta_b$ is the two-point connected correlation function,[45] and it is this function which primarily determines the form of the cross section of incoherent scattering.

Finding F_{ab} [which in the case of epitaxial growth depends on time, i.e., $F_{ab} = F_{ab}(t)$] requires the many-particle distribution function characterizing the nonequilibrium evolution of the growing surface. To evaluate this quantity, we consider an exactly solvable model, namely, the model of local perfect layer growth, which provides a reasonable approximation to the actual evolution of the surface morphology, and for which the many-particle correlation function can be found exactly.[35,36] In this model the surface is divided into square subsections of side length N, each containing N^2 sites. We impose the condition that an atom arriving in a particular subsection must go into the lowest unfilled layer *in that subsection*, and within a particular subsection only two heights may coexist at a given time. Taking into account the fact that subsections are statistically independent and assuming that the rate of deposition is τ^{-1} monolayers per second, the probability of finding L atoms in a given subsection at the time t is given by the Poisson distribution

$$P_L(t) = [(N^2t/\tau)^L/L!]\exp(-N^2t/\tau). \tag{27}$$

To determine the coverage $\Theta_\alpha(t)$ of a particular layer α we note that, according to our definition, *provided that we have L atoms in the subsection*, the probability $p_a(L)$ of finding an atom at the site a belonging to the layer α is

$$p_a(L) = \begin{cases} 0, & \text{when } L \le N^2(\alpha-1)\ , \\ [L - N^2(\alpha-1)]/N^2, & \text{when } N^2(\alpha-1) \le L \le N^2\alpha\ , \\ 1, & \text{when } L \ge N^2\alpha\ . \end{cases}$$

Averaging this over the distribution (27), we obtain

$$\Theta_\alpha(t) = \sum_{l=0}^{\infty} p_a(l)P_l(t)$$
$$= 1 - \sum_{l=0}^{N^2\alpha}[(N^2t/\tau)^l/l!]\exp(-N^2t/\tau) + \sum_{l=1}^{N^2}\left[\frac{(N^2t/\tau)^{N^2(\alpha-1)+l}}{\{N^2(\alpha-1)+l\}!}\right](l/N^2)\exp(-N^2t/\tau). \tag{28}$$

To evaluate the two-site connected correlation function, we need to distinguish between two possibilities, that both the site a and the site b can belong to the same subsection by a suitable location of the subsection, and that a and b are separated in the lateral direction by a distance exceeding the size of a subsection and therefore cannot belong to the same subsection whatever its location. In the latter case $F_{ab}(t) = 0$, due to the statistical independence of different subsections.

Considering two sites belonging to the same subsection, we introduce the coordinates characterizing the position of each site in a three-dimensional crystal lattice: $a = (i_x, i_y, \alpha)$ and $b = (i'_x, i'_y, \beta)$. Having considered three cases $\alpha = \beta$, $\alpha > \beta$, and $\alpha < \beta$, and averaging various configurations with the distribution function (27) as well as taking into account the possibility of an arbitrary choice of the origin, we obtain

$$F_{\mathbf{i}\alpha,\mathbf{i}'\beta}(t) = [\Theta_{\max\{\alpha,\beta\}}(t) - \Theta_\alpha(t)\Theta_\beta(t)]\left(1 - \frac{|i_x - i'_x|}{N}\right)\left(1 - \frac{|i_y - i'_y|}{N}\right)$$
$$+\delta_{\alpha\beta}\sum_{l=1}^{N^2}\left[\frac{(N^2t/\tau)^{N^2(\alpha-1)+l}}{\{N^2(\alpha-1)+l\}!}\right]\left(\frac{l}{N^2}\right)\left(1 - \frac{l-1}{N^2-1}\right)\exp(-N^2t/\tau)$$
$$\times\left[\delta_{\mathbf{ii}'} - \left(1 - \frac{|i_x - i'_x|}{N}\right)\left(1 - \frac{|i_y - i'_y|}{N}\right)\right], \tag{29}$$

where $\delta_{\mathbf{ii}'}$ is the Kronecker delta symbol, and $\max\{\alpha,\beta\}$ denotes the largest of the two integers α and β. As expected, the function $F_{\mathbf{i}\alpha,\mathbf{i}'\beta}(t)$ in (29) vanishes at the edges of a subsection, i.e., if $|i_x - i'_x| = N$ or $|i_y - i'_y| = N$. At each particular time this function can be represented in the form of the four-dimensional array of size $N \times N \times N_l \times N_l$, where N_l is the number of partially filled atomic layers.

In some cases it is more convenient to consider the temporal evolution of a *scalar* quantity which characterizes the morphology of the growing surface, rather than the time dependence of the elements of a large matrix. The *density of steps* was defined in Ref. 52 as a phenomenological scalar parameter, which makes it possible to follow the temporal transformations of the growing surface between flat and rough states, and which was shown to provide a good qualitative (and in some cases even a quantitative; see, e.g., Refs. 18 and 53) approximation to the observable evolution of the specular RHEED intensity. Within the framework of the local perfect layer

growth model this quantity is defined as follows:

$$D = N^{-2}\sum_{n=1}^{N-1}\sum_{l=1}^{N-1}\{[1-\delta(h_{n,l},h_{n,l+1})]+[1-\delta(h_{n,l},h_{n+1,l})]\}$$
$$+N^{-2}\sum_{l=1}^{N-1}[1-\delta(h_{N,l},h_{N,l+1})]+N^{-2}\sum_{n=1}^{N-1}[1-\delta(h_{n,N},h_{n+1,N})], \tag{30}$$

where $h_{n,l}$ is the integer height of a column at position (n,l) on the surface. Averaging of (30) results in

$$D(t) = \frac{4(N-1)}{N}\sum_{\alpha=1}^{\infty}\sum_{l=1}^{N^2}\frac{(N^2t/\tau)^{N^2(\alpha-1)+l}}{\{N^2(\alpha-1)+l\}!}\frac{l}{N^2}\left(1-\frac{l-1}{N^2-1}\right)\exp(-N^2t/\tau)$$
$$+\frac{2}{N}\sum_{\alpha=1}^{\infty}\left[\sum_{l=1}^{N^2}\frac{(N^2t/\tau)^{N^2(\alpha-1)+l}}{\{N^2(\alpha-1)+l\}!}\exp(-N^2t/\tau)\right]\left[1-\sum_{l'=1}^{N^2}\frac{(N^2t/\tau)^{N^2(\alpha-1)+l'}}{\{N^2(\alpha-1)+l'\}!}\exp(-N^2t/\tau)\right]$$
$$+\frac{2}{N}\sum_{\alpha=1}^{\infty}\sum_{l=1}^{N^2}\frac{(N^2t/\tau)^{N^2(\alpha-1)+l}}{\{N^2(\alpha-1)+l\}!}\sum_{l'=1}^{N^2}\frac{(N^2t/\tau)^{N^2(\alpha-1)+l'}}{\{N^2(\alpha-1)+l'\}!}\exp(-2N^2t/\tau)\left(\frac{l+l'}{N^2}-2\frac{ll'}{N^4}\right). \tag{31}$$

In the limiting case $N\to\infty$ the local perfect layer growth model coincides with the perfect layer growth model, in which only one layer is not completely filled at a particular time. In this case formula (31) reduces to $D(t)=4\Theta(t)[1-\Theta(t)]$, where $\Theta(t)$ is the coverage of the growing layer. At the opposite limit $N=1$ we obtain[36]

$$D(t) = 2\left[1-\exp(-2t/\tau)I_0\left(\frac{2t}{\tau}\right)\right], \tag{32}$$

where $I_0(x)$ is the modified Bessel function.

In the following section we apply the results obtained above to the analysis of the temporal evolution of the RHEED pattern.

IV. NUMERICAL RESULTS AND DISCUSSION

We start from the definition of the scattering cross section. It is well known that in order to define the amplitude of scattering one needs to consider the asymptotic behavior of the wave function of the continuous spectrum at large distances from the region occupied by the interaction potential. In a similar way, in order to define the cross section of scattering, we need to consider the asymptotic behavior of the density matrix given by Eq. (15).

The first term on the right-hand side of Eq. (15) describes the *coherent* scattering. For the case of a plane wave incident on the specimen,

$$\Psi_{\rm inc}(\mathbf{r}) = \exp(ik\mathbf{n}_0\cdot\mathbf{r}), \tag{33}$$

the first term on the right-hand side of Eq. (15) is given by (see, e.g., Refs. 54 and 50)

$$\rho_0(\mathbf{r},\mathbf{r}') = \Psi^{(+)}_{k\mathbf{n}_0}(\mathbf{r})[\Psi^{(+)}_{k\mathbf{n}_0}(\mathbf{r}')]^*\ , \tag{34}$$

where $\Psi^{(+)}_{k\mathbf{n}_0}(\mathbf{r})$ is the solution of the Schrödinger equation with the effective non-Hermitian potential

$$\hat{U}_{\rm eff} = \langle\hat{U}\rangle + \langle\delta\hat{U}\langle\hat{G}\rangle\delta\hat{U}\rangle, \tag{35}$$

a method of numerical evaluation of which was considered in Ref. 21. The asymptotic behavior of (34) at large distances from the specimen is given by

$$\rho_0(\mathbf{r},\mathbf{r}') = \mathcal{F}(\mathbf{n},\mathbf{n}_0)\frac{\exp(ikr)}{r}\mathcal{F}^*(\mathbf{n},\mathbf{n}_0)\frac{\exp(-ikr')}{r'}, \tag{36}$$

where each function $\mathcal{F}(\mathbf{n},\mathbf{n}_0)$, representing the amplitude of *coherent* scattering, can be found by carrying out the dynamical RHEED calculations.

To evaluate the asymptotic form of the second term on the right-hand side of Eq. (15) we employ the spectral representation of the Green's function (see the Appendix for the derivation)

$$\langle G(\mathbf{r},\mathbf{r}')\rangle = \int\frac{d^3q}{(2\pi)^3}\frac{\exp(i\mathbf{q}\cdot\mathbf{r})\Psi^{(+)}_{-\mathbf{q}}(\mathbf{r}')}{E_k-E_q+i0}, \tag{37}$$

where $E_k=\hbar^2k^2/2m$ and $E_q=\hbar^2q^2/2m$. The asymptotic form of (37) is

$$\langle G(\mathbf{r},\mathbf{r}')\rangle \sim -\frac{m}{2\pi\hbar^2}\frac{\exp(ikr)}{r}\Psi^{(+)}_{-k\mathbf{n}}(\mathbf{r}'), \tag{38}$$

where $\mathbf{n}=\mathbf{r}/|\mathbf{r}|$. The cross section of scattering is then the sum of two terms, the first being the cross section of multiple *coherent* scattering, and the second one being the cross section of multiple *incoherent* scattering:

$$\frac{d\sigma(\mathbf{n},\mathbf{n}_0)}{do} = |\mathcal{F}(\mathbf{n},\mathbf{n}_0)|^2 + \left(\frac{m}{2\pi\hbar^2}\right)^2$$
$$\times\int\int d\mathbf{R}d\mathbf{R}'\Psi^{(+)}_{-k\mathbf{n}}(\mathbf{R})[\Psi^{(+)}_{-k\mathbf{n}}(\mathbf{R}')]^*$$
$$\times\langle\delta U(\mathbf{R})\delta U(\mathbf{R}')\rangle\rho(\mathbf{R},\mathbf{R}'). \tag{39}$$

There are two processes contributing to the second term on the right-hand side of this equation, namely, diffuse

scattering caused by fluctuations of the lattice site occupation numbers n_a occurring during the growth (disorder diffuse scattering, DDS) and the diffuse scattering resulting from thermal disorder (thermal diffuse scattering, TDS). In this paper we consider the first type of diffuse scattering, no consistent treatment of which has been given so far within the framework of the statistical dynamical diffraction theory.

We consider the initial stage of growth when the disordered surface layer remains relatively thin (this implies explicit limitation on the value of t, for in the local perfect layer growth model the effective interface width increases as $t^{1/2}$ for any finite N) and the probability of incoherent rescattering of electrons by the density fluctuations in the surface layer remains relatively small. In this case, substituting (26) for $\langle \delta U(\mathbf{R}) \delta U(\mathbf{R}') \rangle$ and (34) for $\rho(\mathbf{R}, \mathbf{R}')$ in the second term on the right-hand side of (39), we arrive at the cross section of single diffuse scattering

$$\left[\frac{d\sigma(\mathbf{n}, \mathbf{n}_0)}{do}\right]_{\mathrm{DDS}} = \sum_{a,b} F_{ab} \int d\mathbf{R} d\mathbf{R}' \Psi^{(+)}_{-k\mathbf{n}}(\mathbf{R}) \times [\Psi^{(+)}_{-k\mathbf{n}}(\mathbf{R}')]^* f(\mathbf{R} - \mathbf{R}_a) f(\mathbf{R}' - \mathbf{R}_b) \times \Psi^{(+)}_{k\mathbf{n}_0}(\mathbf{R}) [\Psi^{(+)}_{k\mathbf{n}_0}(\mathbf{R}')]^*, \quad (40)$$

where we have defined the real space representation of the atomic scattering amplitude as $f(\mathbf{r} - \mathbf{R}_a) = -(m/2\pi\hbar^2) U(\mathbf{r} - \mathbf{R}_a)$. In principle, as shown in Ref. 21, Eq. (40) must also be averaged over all the possible thermal displacements $\mathbf{u}_a$ of atoms from their equilibrium positions $\mathbf{R}_a$. However, a simple estimate shows that if we are interested in the differential cross section of incoherent scattering through relatively small angles (of the order of the Bragg angle), this averaging has almost no effect on the computed intensity distribution.

It should be emphasized that in accordance with our proof (20), formula (40) is consistent with Eq. (12) in the sense that the total cross section of scattering can be evaluated either by integrating (40) over all directions of $\mathbf{n}$, or by evaluating the rate of "absorption" of electrons by the non-Hermitian part of the effective potential in the Schrödinger equation for $\Psi^{(+)}_{k\mathbf{n}_0}(\mathbf{R})$ [see, e.g., Eq. (16) of Ref. 21]. The second method appears to be less demanding computationally, and we will follow this approach in order to estimate the relative contributions of DDS and TDS to the total cross section of incoherent scattering.

In $\mathbf{q}$ space the effective non-Hermitian potential (35) can be represented in the form of a sum of three terms,[21]

$$\hat{U}_{\mathrm{eff}} = \langle \hat{U} \rangle + \hat{U}^{(\mathrm{TDS})} + \hat{U}^{(\mathrm{DDS})}. \quad (41)$$

The first term is the ordinary interaction between the fast electron and the atoms of the crystal averaged over all the statistical configurations, viz.,

$$\langle U(\mathbf{q}, \mathbf{q}') \rangle = -\frac{2\pi\hbar^2}{m} \sum_a \Theta_a f_a(\mathbf{q} - \mathbf{q}') \times \exp[-i(\mathbf{q} - \mathbf{q}') \cdot \mathbf{R}_a] \times \exp[-M_a(\mathbf{q} - \mathbf{q}')], \quad (42)$$

where $f_a(\mathbf{q})$ is the Born electron-atom scattering amplitude and $\exp[-M_a(\mathbf{q})] = \exp\left[-\langle (\mathbf{q} \cdot \mathbf{u})^2 \rangle_T / 2\right]$ is the Debye-Waller factor.

The second term results from the thermal motion of atoms, viz.,

$$U^{(\mathrm{TDS})}(\mathbf{q}, \mathbf{q}') = -i\frac{\hbar^2}{m} \sum_a \Theta_a^2 \int d\mathbf{Q} f_a(\mathbf{q} - \mathbf{Q}) f_a(\mathbf{Q} - \mathbf{q}') \delta(\mathbf{Q}^2 - k^2) \exp[-i(\mathbf{q} - \mathbf{q}') \cdot \mathbf{R}_a] \times \{\exp[-M_a(\mathbf{q} - \mathbf{q}')] - \exp[-M_a(\mathbf{q} - \mathbf{Q})] \exp[-M_a(\mathbf{q}' - \mathbf{Q})]\}. \quad (43)$$

The third term arises as a result of statistical disorder in the distribution of atoms over the lattice sites,[55] viz.,

$$U^{(\mathrm{DDS})}(\mathbf{q}, \mathbf{q}') = -i\frac{\hbar^2}{m} \sum_a (\Theta_a - \Theta_a^2) \int d\mathbf{Q} f_a(\mathbf{q} - \mathbf{Q}) f_a(\mathbf{Q} - \mathbf{q}') \times \exp[-i(\mathbf{q} - \mathbf{q}') \cdot \mathbf{R}_a] \exp[-M_a(\mathbf{q} - \mathbf{q}')] \delta(\mathbf{Q}^2 - k^2). \quad (44)$$

Note that this term does not appear in models where each atomic potential is assumed to depend on time via a deterministic factor $\Theta_a(t)$.[11,12] To evaluate $\hat{U}^{(\mathrm{TDS})}$ and $\hat{U}^{(\mathrm{DDS})}$ numerically, one needs to perform two-dimensional integration over the entire solid angle of 4π as described by Bird and King.[56] For the purpose of numerical evaluation of $\Psi^{(+)}_{k\mathbf{n}_0}(\mathbf{R})$ and $\Psi^{(+)}_{-k\mathbf{n}}(\mathbf{R})$ it is more convenient to use the Doyle-Turner representation of the effective interaction potential, which consists of an analytical fit to the atomic scattering factor of the form

$$f(s) = \sum_j a_j \exp(-b_j s^2), \quad (45)$$

where $s = q/4\pi$. In real space the potential of a single atom can be expressed in terms of a set of coefficients $\{a_j, b_j\}$ as

$$U(\mathbf{r}) = -\frac{2\pi\hbar^2}{m_0} \sum_j a_j \left(\frac{4\pi}{b_j}\right)^{3/2} \exp(-4\pi^2 \mathbf{r}^2 / b_j), \quad (46)$$

where m_0 is the electron rest mass. In the present study we used the following representation for $f(s)$:

$$f^{(\mathrm{eff})}(s) = \Theta \sum_{j=1}^{5} a_j^{(\mathrm{Re})} \exp(-[b_j^{(\mathrm{Re})} + \mu] s^2) + i\Theta^2 \sum_{j=1}^{3} a_j^{(\mathrm{TDS})} \exp(-[b_j^{(\mathrm{TDS})} + \mu/2] s^2) + i(\Theta - \Theta^2) \sum_{j=1}^{3} a_j^{(\mathrm{DDS})} \exp(-[b_j^{(\mathrm{DDS})} + \mu] s^2), \quad (47)$$

TABLE I. The coefficients of the Doyle-Turner expansion (47) for atomic As and Ga for $E = 14$ keV and $T = 800$ K.

j	$a_{\mathrm{As}}^{(\mathrm{Re})}$ Å	$a_{\mathrm{As}}^{(\mathrm{TDS})}$ Å	$a_{\mathrm{As}}^{(\mathrm{DDS})}$ Å	$b_{\mathrm{As}}^{(\mathrm{Re})}$ Å^2	$b_{\mathrm{As}}^{(\mathrm{TDS})}$ Å^2	$b_{\mathrm{As}}^{(\mathrm{DDS})}$ Å^2
1	2.236807	0.378741	1.013115	47.638923	2.902726	2.967957
2	2.839050	0.644963	0.967085	13.820734	1.396553	0.327727
3	1.445425	-0.091111	0.285496	2.673381	0.184380	0.023353
4	0.637972	0.0	0.0	0.619943	0.0	0.0
5	0.153667	0.0	0.0	0.071465	0.0	0.0
j	$a_{\mathrm{Ga}}^{(\mathrm{Re})}$ Å	$a_{\mathrm{Ga}}^{(\mathrm{TDS})}$ Å	$a_{\mathrm{Ga}}^{(\mathrm{DDS})}$ Å	$b_{\mathrm{Ga}}^{(\mathrm{Re})}$ Å^2	$b_{\mathrm{Ga}}^{(\mathrm{TDS})}$ Å^2	$b_{\mathrm{Ga}}^{(\mathrm{DDS})}$ Å^2
1	2.131248	0.268100	0.899768	69.589595	3.317216	2.584799
2	2.512511	0.667653	0.831471	17.413796	1.314195	0.309689
3	1.605124	-0.114010	0.245848	3.170213	0.224565	0.022662
4	0.691159	0.0	0.0	0.704249	0.0	0.0
5	0.156772	0.0	0.0	0.076906	0.0	0.0

where $\mu = 8\pi^2\langle u^2\rangle$. All the parameters $\{a_j, b_j\}$ entering (47) have been determined by Levenberg-Marquardt fitting[57] to the Doyle-Turner form of data taken either from the *International Tables for x-ray Crystallography*[58] or evaluated by two-dimensional integration of (43) and (44). The results obtained for Ga and As atoms are summarized in Table I (note that the coefficients $a_j^{(\mathrm{TDS})}$ and $b_j^{(\mathrm{TDS})}$ are temperature dependent, while the other coefficients are not).

As follows from (43) and (44), the effective interaction $\hat{U}^{(\mathrm{eff})}$ is periodic within any plane parallel to the initially flat surface of the crystal and so can be expanded as a two-dimensional Fourier series $U^{(\mathrm{eff})}(\mathbf{r}) = \sum_{\mathbf{g}} U_{\mathbf{g}}(z)\exp(i\mathbf{g}\cdot\mathbf{x})$, where $\mathbf{g}$ is a two-dimensional reciprocal lattice vector and $\mathbf{x} = (x, y)$. Each of the wave functions $\Psi_{k\mathbf{n}_0}^{(+)}(\mathbf{R})$ and $\Psi_{-k\mathbf{n}}^{(+)}(\mathbf{R})$ can be represented in a similar form as two-dimensional Bloch functions,

$$\Psi_{k\mathbf{n}_0}^{(+)}(\mathbf{R}) = \sum_{\mathbf{g}} \Phi_{\mathbf{g}}^{(0)}(z)\exp\{i[k(\mathbf{n}_0)_{\parallel} + \mathbf{g}]\cdot\mathbf{x}\}, \quad (48)$$

resulting in a system of coupled second-order differential equations for the functions $\Phi_{\mathbf{g}}^{(0)}(z)$. This system of equations in most cases has to be studied numerically, and two types of approximation have in the past been employed. One[59] requires the expansion (48) to include as many terms as possible (e.g., more than a hundred), while the other (see, e.g., Refs. 11 and 60) is essentially a one-dimensional approximation, i.e., it includes only one term of the series (48), namely, $\Phi_0^{(0)}(z)$. In principle the first approach should be followed, but in many cases this involves substantial computation which sometimes hinders a qualitative understanding of the results obtained. The second approach has the serious disadvantage of being basically *qualitative*, and, in particular, does not take into account the phenomenon of the resonance scattering.[61–64] However, numerical implementation of this technique is far simpler, which is particularly advantageous if, as here, a preliminary analysis of dynamical effects has to be performed. All the results described below have been obtained using this one-dimensional approximation $\Psi_{k\mathbf{n}_0}^{(+)}(\mathbf{R}) = \Phi_0^{(0)}(z)\exp[ik(\mathbf{n}_0)_{\parallel}\cdot\mathbf{x}]$, which was described in detail in Refs. 11 and 60.

We start from an evaluation of the total diffuse scattering cross section. Following Mott and Massey,[65] we express the total current of diffusely scattered electrons in terms of the imaginary part of the effective interaction potential as

$$\int_{\Sigma} d\mathbf{a}\,(\mathbf{j}^{(\mathrm{DDS})} + \mathbf{j}^{(\mathrm{TDS})}) = -\frac{2}{\hbar}\int_V d\mathbf{r}\,\mathrm{Im}U^{(\mathrm{eff})}(\mathbf{r})|\Psi_{k\mathbf{n}}^{(+)}(\mathbf{r})|^2. \quad (49)$$

In the case of one-dimensional diffraction the diffuse scattering cross section per unit surface area is

$$\sigma_{\mathrm{tot}}^{(\mathrm{DDS})} = (Av\sin\zeta_0)^{-1}\int_{\Sigma} d\mathbf{a}\,\mathbf{j}^{(\mathrm{DDS})} = -\frac{2m}{\hbar^2 k\sin\zeta_0}\int_{-\infty}^{\infty} dz\,U^{(\mathrm{DDS})}(z)|\Phi_0^{(0)}(z)|^2\,, \quad (50)$$

where ζ_0 is the grazing angle and A is the area of the surface. Taking into account the conservation law (24), we obtain that $|R|^2 + \sigma_{\mathrm{tot}}^{(\mathrm{DDS})} + \sigma_{\mathrm{tot}}^{(\mathrm{TDS})} = 1$, where $|R|^2$ is the coherent intensity. This equality makes it possible to evaluate the relative contributions of diffuse and thermal diffuse scattering to the total incoherent scattering cross section for any particular value of ζ_0, avoiding the necessity of carrying out direct numerical integration of the second term on the right-hand side of Eq. (39) over the entire solid angle 4π. Figure 7 shows the dependence of the coherent intensity $|R|^2$ and the cross sections $\sigma_{\mathrm{tot}}^{(\mathrm{DDS})}$ and $\sigma_{\mathrm{tot}}^{(\mathrm{TDS})}$ on the grazing angle ζ_0 at various times. As follows from the results shown in Fig. 7, in the region where the surface reflectivity is appreciable the TDS cross section ($\sigma_{\mathrm{tot}}^{(\mathrm{TDS})}$) is almost insensitive to the conditions existing at the surface, and the coherent intensity varies in antiphase with respect to $\sigma_{\mathrm{tot}}^{(\mathrm{DDS})}$. This points clearly to the fact that it is the variation of the surface morphology which is largely responsible for oscillations of the specular RHEED intensity in the

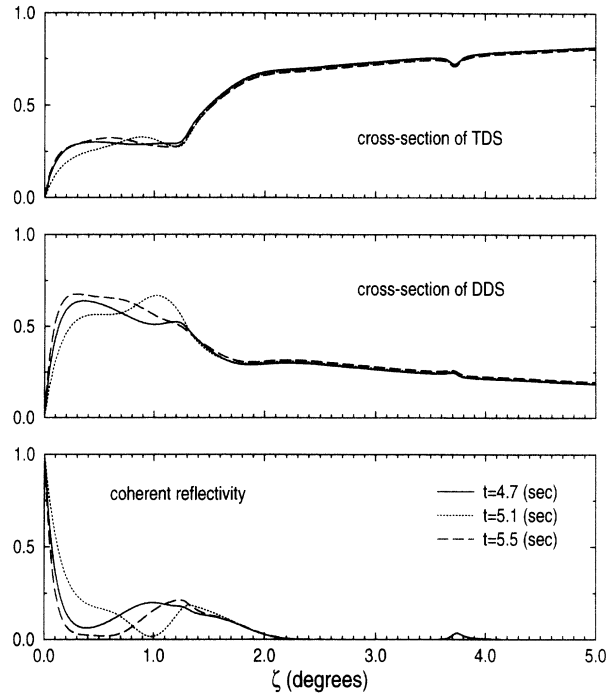

FIG. 7. The probabilities for various channels of scattering versus the grazing angle of incidence for a singular GaAs (001) surface. The parameters are $T = 800$ K, $N^2 = 16$, $E = 14$ keV, and $\tau^{-1} = 1$ ML/s^{-1}.

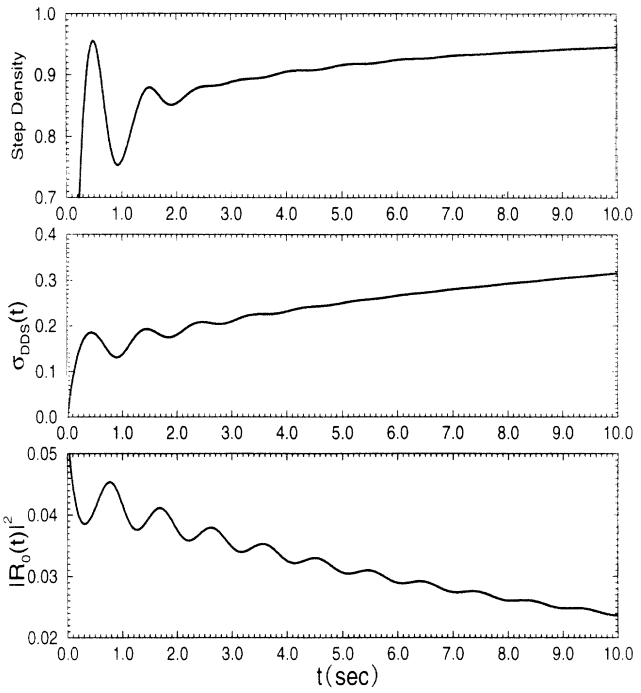

FIG. 8. Temporal evolution of the step density, the cross section $\sigma_{\rm DDS}$ of the disorder diffuse scattering, and the specular (coherent) intensity $|R_0|^2$ for the GaAs (001) singular surface. The parameters are $T = 800$ K, $N^2 = 16$, $E = 14$ keV, and $\zeta_0 = 3.72°$.

vicinity of the Bragg conditions of incidence (i.e., where the *coherent* part of the surface reflectivity is sufficiently large).

To understand this in more detail, we analyzed the temporal evolution of the coherent intensity $|R|^2$ and the diffuse scattering cross section $\sigma_{\rm tot}^{\rm (DDS)}$ for the (008) Bragg condition, where the peak of the reflectivity at $E = 14$ keV corresponds to $\zeta_0 = 3.72°$. The results obtained for two different sizes of a subsection are depicted in Figs. 8 and 9. For comparison, the upper curve in each figure shows the temporal evolution of the step density (31), and there is an apparent similarity between the curves describing the dependence of the diffuse scattering cross section $\sigma_{\rm tot}^{\rm (DDS)}(t)$ and the density of steps $D(t)$. It should be emphasized that elimination of the contribution of the diffuse scattering [i.e. the term (44)] from the effective interaction potential $\hat{U}^{\rm (eff)}$ changes the phase of the oscillations of $|R(t)|^2$ by π and there remains no similarity between the behavior of $|R(t)|^2$ and $-D(t)$.

A possible explanation of this phenomenon (note that the existence of a strong correlation between the temporal evolution of the specular intensity and the density of steps for the Bragg conditions of incidence has been observed recently; see, e.g., Refs. 18 and 53) can be obtained by analyzing the form of the standing wave pattern, i.e. the inhomogeneous distribution of the density of high-energy electrons in the vacuum. This distribution appears as a result of interference between the incident wave and the wave reflected from the crystal surface, the

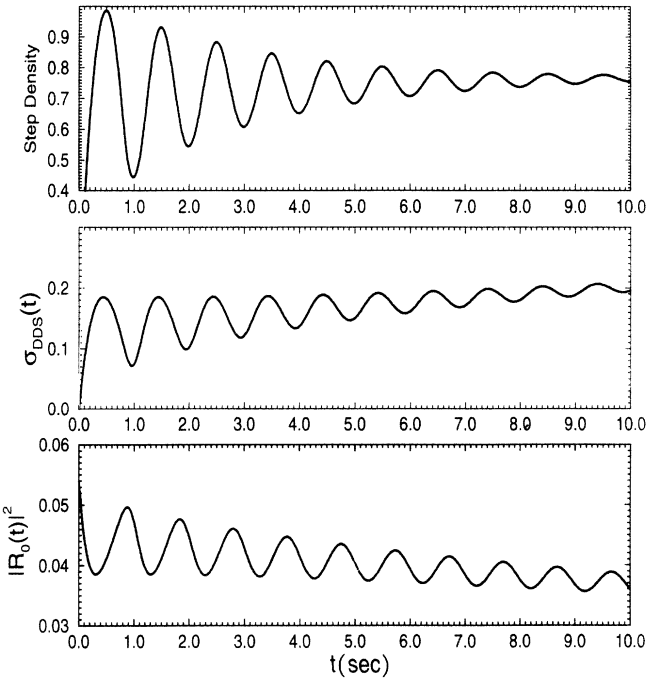

FIG. 9. Same as for Fig. 8 except that $N^2 = 64$.

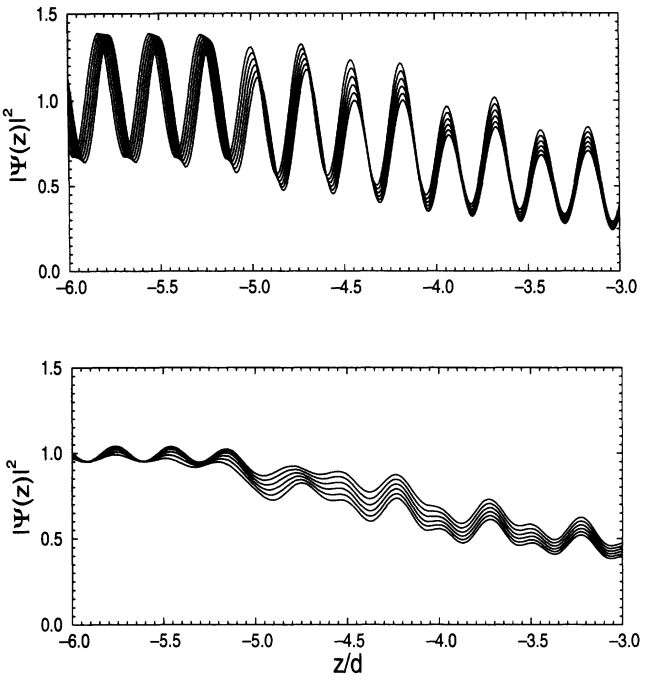

FIG. 10. The distribution of probability density in the one-dimensional standing wave pattern. The upper curves correspond to the Bragg condition of incidence $\zeta_0 = 3.72°$ (i.e., there is a peak in the surface reflectivity at $\zeta_0 = 3.72°$). The lower curves show the structure of the standing wave pattern existing for the angle of incidence which is far away from the Bragg condition. Six curves shown in each figure correspond to t =4.0, 4.1, ... , 4.5 s, and $\tau^{-1} = 1$ ML/s^{-1}.

effect of which was discussed by Peng and Cowley.[66] For $\zeta_0 = 3.72°$ this standing wave (the upper curve in Fig. 10) has intensity maxima in the vicinity of centers of unfilled atomic layers [the GaAs(001) surface consists of consecutively distributed layers of Ga and As atoms occupying the positions $z_{\mathrm{As}} = Md$ and $z_{\mathrm{Ga}} = (M + 1/2)d$, where M is an integer and $d = 1.41$ Å]. In the crystal bulk, the corresponding solution $\Psi^{(+)}_{\mathbf{kn}_0}(\mathbf{R})$ has intensity minima in the vicinity of atomic planes, resulting in a substantial decrease in the probability of phonon scattering (the so-called "anomalous transmission" effect[67]), and in an increase in the cross section of diffuse scattering by fluctuations of the lattice site occupation numbers occurring in the growing layer.

It is important to emphasize that standing waves of the form shown in Fig. 10 arise not only in the initial state of scattering, but in the *final* state as well. This follows from the apparent symmetry of formula (40) with respect to the rearrangement $\mathbf{n}_0 \leftrightarrow -\mathbf{n}$. In particular, the wave function of the final state $\Psi^{(+)}_{-\mathbf{kn}}(\mathbf{R})$, corresponding to the grazing angle of scattering $\zeta_{\mathrm{scatt}} = 3.72°$, has exactly the same form as the wave function shown in the upper part of Fig. 10. Arguments similar to those discussed above indicate that we can expect not only some relative enhancement of $\sigma^{(\mathrm{DDS})}_{\mathrm{tot}}$ in the vicinity of $\zeta_0 = 3.72°$, but also some enhancement in the *differential* scattering cross section for $\zeta_{\mathrm{scatt}} \approx 3.72°$.

Equation (40) shows that in order to calculate the differential scattering cross section, we need to evaluate the two-dimensional Fourier transform of the correlation function (29). Performing summation over the lattice sites, we arrive at

$$
\begin{aligned}
F_{\alpha\beta}(\mathbf{q}_{\|}) = {} & \delta_{\alpha\beta} \sum_{l=1}^{N^2} \left[\frac{(N^2 t/\tau)^{N^2(\alpha-1)+l}}{\{N^2(\alpha-1)+l\}!} \right] \left(\frac{l}{N^2} \right) \left(1 - \frac{l-1}{N^2-1} \right) \exp(-N^2 t/\tau) \\
& + \left[1 + 2 \sum_{j=1}^{N} (1 - j/N) \cos[(\mathbf{q}_{\|})_x a j] \right] \left[1 + 2 \sum_{j=1}^{N} (1 - j/N) \cos[(\mathbf{q}_{\|})_y a j] \right] \\
& \times \Bigg\{ \Theta_{\max\{\alpha,\beta\}}(t) - \Theta_{\alpha}(t)\Theta_{\beta}(t) \\
& - \delta_{\alpha\beta} \sum_{l=1}^{N^2} \left[\frac{(N^2 t/\tau)^{N^2(\alpha-1)+l}}{\{N^2(\alpha-1)+l\}!} \right] \left(\frac{l}{N^2} \right) \left(1 - \frac{l-1}{N^2-1} \right) \exp(-N^2 t/\tau) \Bigg\},
\end{aligned}
\tag{51}
$$

where a is the period of the crystal lattice in the lateral direction. The first term on the right-hand side of (51) does not depend on $\mathbf{q}_{\|}$ and describes the homogeneous background of diffusely scattered electrons. The second term can be evaluated using the Euler-Maclaurin summation formula,[68] $\sum_{j=1}^{N}(1 - j/N)\cos(jqa) \approx 2[1 - \cos(qaN)]/N(qa)^2$, and exhibits a notable maximum in the vicinity of $\mathbf{q}_{\|} = \mathbf{0}$. This maximum exists at any value ζ_{scatt} and appears as a vertical streak in the angular distribution of the diffusely scattered electrons. This streak is distinguishable in Fig. 11, where the distribution of incoherently scattered electrons is plotted as a function of azimuthal and grazing angles for a coverage of half a monolayer. The bright horizontal lines in Fig. 11 are the horizontal (004) and (008) Kikuchi lines which result from the aforementioned effect of formation of the standing wave pattern in the final state of the scattering process.

An interesting question concerns the temporal evolution of the pattern shown in Fig. 11. In Fig. 12 three curves are shown representing the distribution of the diffuse intensity along the streak corresponding to $\mathbf{q}_{\|} = \mathbf{0}$ at various times with increasing surface disorder. As follows from the results shown in Fig. 12, it is the (008)

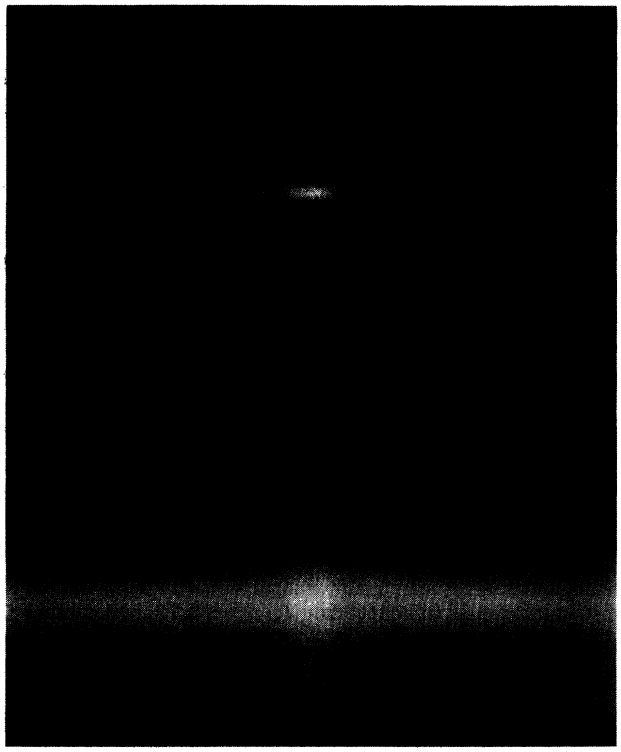

FIG. 11. The distribution of the diffuse intensity computed using the one-dimensional approximation for half a monolayer coverage ($t = 0.5\tau$) for $N^2 = 64$. A bright narrow horizontal line in the upper part of the figure is the (008) Kikuchi line, while the relatively broad enhancement of intensity at the bottom of the figure corresponds to the (004) forbidden gap in the one-dimensional band structure for the (001) row of reflections.

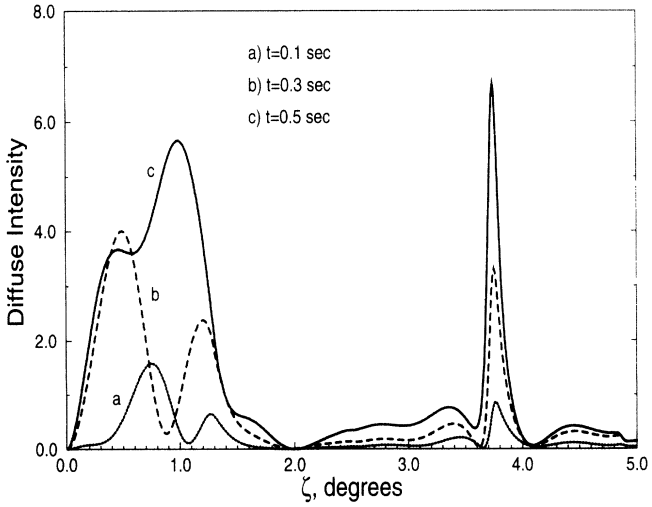

FIG. 12. The distribution of the diffuse intensity scattered from the GaAs (001) surface along the (00) two-dimensional reciprocal lattice rod at various times with $\tau^{-1} = 1$ ML/s^{-1} and $N^2 = 16$. The grazing angle of incidence is $\zeta_0 = 4.5°$, and the intensity of the coherent specular reflection is artificially reduced.

horizontal Kikuchi line which exhibits the strongest increase of intensity when the layer coverage reaches the value of $\Theta = 0.5$. Behaviour of the Kikuchi line intensity similar to that shown in Fig. 12 has been observed and discussed by Zhang *et al.*[23] Note that the angle of incidence has been chosen to be $\zeta_0 = 4.5°$, so that the position of the (008) Kikuchi line is closer to the position of the specular beam (the intensity of which is artificially reduced) than to the position of any other Kikuchi line in the RHEED pattern, this configuration being very similar to the diffraction conditions used by Zhang *et al.*[23]. At the same time it should be noted that the intensity of the diffuse streak shown in Figs. 11 and 12 is lower than that observed experimentally, which probably results from the long-range correlations and/or delocalized excitations which exist at the real surface of a crystal.

V. CONCLUSIONS

In summary, we have formulated a statistical multiple scattering approach to the problem of dynamical diffraction of high-energy electrons from a growing surface of a crystal. Our approach is based on the diagram technique, representing a regular way of evaluating the perturbation expansions for the states of the continuous spectrum. We have found explicit expressions for the *coherent* and *incoherent* scattering cross sections, and have applied the theory to the analysis of the effects of short-range order and its influence on the RHEED pattern.

We believe that the method described above provides a relatively simple description of the basic phenomena characterizing reflection diffraction of high-energy electrons (RHEED) from a statistically disordered growing surface, and this can help in the realization of the full potential of this diffraction technique for studying the kinetics of the atomic growth processes.

ACKNOWLEDGMENTS

The authors acknowledge valuable discussions with Professor G. Meyer-Ehmsen and Dr. L.-M. Peng. S.L.D. was supported by the Science and Engineering Research Council (SERC), Grant No. GR/H96423. D.D.V. was supported by Imperial College and the Research Development Corporation of Japan through the "Atomic Arrangement: Design and Control for New Materials" Joint Research Program. Numerical computations were performed at the Materials Modelling Laboratory, Department of Materials, University of Oxford, which is partly funded by the SERC (Grant No. GR/H58278).

APPENDIX

In this Appendix we derive representation (37) for the Green's function of the high-energy electron [for the purpose of the derivation we will use the notation $\mathcal{G}$ for the Green's function, which may not coincide with (5)]. This function

$$\hat{\mathcal{G}} = \frac{1}{E - \hat{K} - \hat{U} + i0} \tag{A1}$$

can be represented by an infinite series of the form

$$\hat{\mathcal{G}} = \hat{\mathcal{G}}_0 + \hat{\mathcal{G}}_0\hat{U}\hat{\mathcal{G}}_0 + \hat{\mathcal{G}}_0\hat{U}\hat{\mathcal{G}}_0\hat{U}\hat{\mathcal{G}}_0 + \cdots, \tag{A2}$$

where

$$\hat{\mathcal{G}}_0 = \frac{1}{E - \hat{K} + i0}. \tag{A3}$$

In real space $\hat{\mathcal{G}}_0 = \mathcal{G}_0(\mathbf{r}, \mathbf{r}')$ can be written as

$$\mathcal{G}_0(\mathbf{r}, \mathbf{r}') = \int \frac{d^3q}{(2\pi)^3} \frac{\exp[i\mathbf{q}\cdot(\mathbf{r} - \mathbf{r}')]}{E - E_q + i0} = -\frac{m}{2\pi\hbar^2} \frac{\exp(ik|\mathbf{r} - \mathbf{r}'|)}{|\mathbf{r} - \mathbf{r}'|}, \tag{A4}$$

where $E_q = \hbar^2 q^2/2m$. By definition, the function $\Psi^{(+)}$ is the sum of the series

$$\Psi^{(+)} = \phi + \hat{\mathcal{G}}_0\hat{U}\phi + \hat{\mathcal{G}}_0\hat{U}\hat{\mathcal{G}}_0\hat{U}\phi + \cdots, \tag{A5}$$

where ϕ represents the incident wave. Introducing the operator

$$\hat{\mathcal{P}} = 1 + \hat{\mathcal{G}}_0\hat{U} + \hat{\mathcal{G}}_0\hat{U}\hat{\mathcal{G}}_0\hat{U}\cdots, \tag{A6}$$

we can write explicitly for (A5) and (A2)

$$\Psi_{\mathbf{q}}^{(+)}(\mathbf{r}) = \int d^3r''\mathcal{P}(\mathbf{r}, \mathbf{r}'')\exp(i\mathbf{q}\cdot\mathbf{r}''), \tag{A7}$$

and

$$\mathcal{G}(\mathbf{r}, \mathbf{r}') = \int d^3r''\mathcal{P}(\mathbf{r}, \mathbf{r}'')\mathcal{G}_0(\mathbf{r}'', \mathbf{r}'). \tag{A8}$$

Substituting (A4) into (A8) we arrive at

$$\mathcal{G}(\mathbf{r}, \mathbf{r}') = \int d^3r''\mathcal{P}(\mathbf{r}, \mathbf{r}'') \int \frac{d^3q}{(2\pi)^3} \frac{\exp[i\mathbf{q}\cdot(\mathbf{r}'' - \mathbf{r}')]}{E - E_q + i0}. \tag{A9}$$

Using Eq. (A7), we transform (A9) as follows:

$$\mathcal{G}(\mathbf{r}, \mathbf{r}') = \int \frac{d^3q}{(2\pi)^3} \frac{\Psi_{\mathbf{q}}^{(+)}(\mathbf{r})\exp(-i\mathbf{q}\cdot\mathbf{r}')}{E - E_q + i0}. \tag{A10}$$

Using the symmetry property of the Green's function $\mathcal{G}(\mathbf{r}, \mathbf{r}') = \mathcal{G}(\mathbf{r}', \mathbf{r})$ and changing the variable of integration $\mathbf{q} \to -\mathbf{q}$, we arrive at (37). Note that in our derivation we did not assume the operator $\hat{U}$ to be Hermitian, so that formulas (A10) and (37) are valid for the general case of a non-Hermitian and nonlocal interaction potential.

[1] B. A. Joyce, Rep. Prog. Phys. **48**, 1637 (1985).
[2] B. A. Joyce, N. Ohtani, S. M. Mokler, T. Shitara, J. Zhang, J. H. Neave, and P. N. Fawcett, Surf. Sci. **298**, 399 (1993).
[3] J. J. Harris, B. A. Joyce, and P. J. Dobson, Surf. Sci. **103**, L90 (1981); **108**, L444 (1981).
[4] J. M. Van Hove, C. S. Lent, P. R. Pukite and P. I. Cohen, J. Vac. Sci. Technol. B **1**, 741 (1983).
[5] J. H. Neave, B. A. Joyce, P. J. Dobson, and N. Norton, Appl. Phys. A **31**, 1 (1983).
[6] C. S. Lent and P. I. Cohen, Surf. Sci. **139**, 121 (1984).
[7] T. Kawamura and P. A. Maksym, Surf. Sci. **161**, 12 (1985).
[8] C. S. Lent and P. I. Cohen, Phys. Rev. B **33**, 8329 (1986).
[9] A. Ichimiya, Surf. Sci. **187**, 194 (1987).
[10] H. Toyoshima, T. Shitara, J. Zhang, J. H. Neave, and B. A. Joyce, Surf. Sci. **264**, 10 (1992).
[11] L.-M. Peng and M. J. Whelan, Surf. Sci. **238**, L446 (1990); Proc. R. Soc. London Ser. A **432**, 195 (1991); **435**, 257 (1991); **435**, 269 (1991).
[12] Z. Mitura, A. Daniluk, M. Strózak, M. Jalochowski, A. Smal, and M. Subotowicz, Acta Phys. Pol. A **80**, 365 (1991); Z. Mitura, M. Strózak, and M. Jalochowski, Surf. Sci. **276**, L15 (1992).
[13] P. I. Cohen, G. S. Petrich, P. R. Pukite, G. J. Whaley, and A. S. Arrott, Surf. Sci. **216**, 222 (1989).
[14] B. A. Joyce, J. H. Neave, P. J. Dobson, and P. K. Larsen, Phys. Rev. B **29**, 814 (1984).
[15] B. A. Joyce, P. J. Dobson, J. H. Neave, and J. Zhang, Surf. Sci. **174**, 1 (1986).
[16] B. A. Joyce, P. J. Dobson, J. H. Neave, and J. Zhang, Surf. Sci. **178**, 110 (1986).
[17] T. Shitara, D. D. Vvedensky, M. R. Wilby, J. Zhang, J. H. Neave, and B. A. Joyce, Appl. Phys. Lett. **60**, 1504 (1992).
[18] T. Shitara, D. D. Vvedensky, M. R. Wilby, J. Zhang, J. H. Neave, and B. A. Joyce, Phys. Rev. B **46**, 6815 (1992).
[19] T. Shitara, D. D. Vvedensky, M. R. Wilby, J. Zhang, J. H. Neave, and B. A. Joyce, Phys. Rev. B **46**, 6825 (1992).
[20] A. Ichimiya, Acta Crystallogr. Sect. A **44**, 1042 (1988).
[21] S. L. Dudarev, L.-M. Peng, and M. J. Whelan, Surf. Sci. **279**, 380 (1992).
[22] G. Meyer-Ehmsen, B. Bölger, and P. K. Larsen, Surf. Sci. **224**, 591 (1989).
[23] J. Zhang, J. H. Neave, P. J. Dobson, and B. A. Joyce, Appl. Phys. A **42**, 317 (1987).
[24] P. K. Larsen, G. Meyer-Ehmsen, B. Bölger, and A.-J. Hoeven, J. Vac. Sci. Technol. A **5**, 611 (1987).
[25] P. K. Larsen and G. Meyer-Ehmsen, Surf. Sci. **240**, 168 (1990).
[26] P. I. Cohen, P. R. Pukite, and S. Batra, in *Thin Film Growth Techniques for Low-Dimensional Structures*, Vol. 163 of *NATO Advanced Study Institute, Series B: Physics*, edited by R. F. C. Farrow, S. S. P. Parkin, P. J. Dobson, J. H. Neave, and A. S. Arrott (Plenum Press, New York, 1986), pp. 69–94.
[27] G. Lehmpfuhl, A. Ichimiya, and H. Nakahara, Surf. Sci. **245**, L159 (1991).
[28] U. Korte and G. Meyer-Ehmsen, Surf. Sci. **277**, 109 (1992).
[29] U. Korte, Ph.D. dissertation, Universität Osnabrück, 1992.
[30] U. Korte and G. Meyer-Ehmsen, Phys. Rev. B **48**, 8345 (1993).
[31] S. Clarke and D. D. Vvedensky, Phys. Rev. Lett. **58**, 2235

(1987).
[32]D. D. Vvedensky, S. Clarke, and M. R. Wilby, Prog. Surf. Sci. **35**, 87 (1991).
[33]D. D. Vvedensky, N. Haider, T. Shitara, and P. Šmilauer, Philos. Trans. R. Soc. London Ser. A **344**, 493 (1993).
[34]D. D. Vvedensky, A. Zangwill, C. N. Luse, and M. R. Wilby, Phys. Rev. E **48**, 852 (1993).
[35]A. K. Myers-Beaghton and D. D. Vvedensky, J. Phys. A **22**, L467 (1989).
[36]A. K. Myers-Beaghton and D. D. Vvedensky, Surf. Sci. **232**, 161 (1990).
[37]A. K. Myers-Beaghton and D. D. Vvedensky, Phys. Rev. B **42**, 5544 (1990).
[38]A. K. Myers-Beaghton and D. D. Vvedensky, Phys. Rev. B **44**, 2457 (1991).
[39]S. F. Edwards, Philos. Mag. **3**, 1020 (1958).
[40]A. A. Abrikosov, L. P. Gorkov, and I. E. Dzyaloshinskii, *Methods of Quantum Field Theory in Statistical Physics* (Dover, New York, 1975), p. 329.
[41]U. Frisch, in *Probabilistic Methods in Applied Mathematics*, edited by A. T. Bharucha-Reid (Academic Press, New York, 1968), p. 75.
[42]A. Ishimaru, *Wave Propagation and Scattering in Random Media* (Academic Press, New York, 1978).
[43]V. Holý and K. T. Gabrielyan, Phys. Status Solidi **140**, 39 (1987).
[44]H. Drescher, L. Reimer, and H. Seidel, Z. Angew. Phys. **29**, 331 (1970).
[45]J. J. Binney, N. J. Dowrick, A. J. Fisher, and M. E. J. Newman, *The Theory of Critical Phenomena* (Clarendon Press, Oxford, 1992), p. 43.
[46]K. Blum, *Density Matrix: Theory and Applications* (Plenum Press, New York, 1981).
[47]S. L. Dudarev, L.-M. Peng, and M. J. Whelan, Phys. Lett. A **170**, 111 (1992); Proc. R. Soc. London Ser. A **440**, 567 (1993).
[48]S. L. Dudarev, L.-M. Peng, and M. J. Whelan, Phys. Rev. B **48**, 13 408 (1993).
[49]The effective radius of screening of the potential of an atom can be estimated using the Thomas-Fermi model (Ref. 50) as $r_{\rm scr} \approx 0.885\hbar^2/me^2Z^{1/3}$, where Z is the number of electrons. With higher precision this radius can be evaluated by analyzing the behavior of the cross section of elastic scattering, namely, $r_{\rm scr} = \lambda/4\pi\sqrt{B}$, where B is a fitting parameter introduced by Riley *et al.* (Ref. 51).
[50]L. D. Landau and E. M. Lifshitz, *Quantum Mechanics, Non-Relativistic Theory*, 3rd ed. (Pergamon Press, Oxford, 1977).
[51]M. E. Riley, C. J. MacCallum, and F. Biggs, At. Data Nucl. Data Tables **15**, 443 (1975); **28**, 379 (1983).
[52]D. D. Vvedensky and S. Clarke, Surf. Sci. **225**, 373 (1990).
[53]P. Šmilauer, M. R. Wilby, and D. D. Vvedensky, Phys. Rev. B **48**, 4968 (1993).
[54]M. Goldberger and K. M. Watson, *Collision Theory* (Wiley, New York, 1967).
[55]A. Howie and R. M. Stern, Z. Naturforsch. Teil A **27**, 382 (1972).
[56]D. M. Bird and Q. A. King, Acta Crystallogr. Sect. A **46**, 202 (1990).
[57]W. H. Press, S. A. Teukolsky, W. A. Vetterling, and B. A. Flannery, *Numerical Recipes in FORTRAN*, 2nd ed. (Cambridge University Press, Cambridge, 1992), p. 678.
[58]*International Tables for X-ray Crystallography* (Kynoch Press, Birmingham, 1962), Vol. III, p. 152.
[59]J. M. McCoy, U. Korte, P. A. Maksym, and G. Meyer-Ehmsen, Surf. Sci. **261**, 29 (1992).
[60]A. Ichimiya, S. Kohmoto, H. Nakahara, and Y. Horio, Ultramicroscopy **48**, 425 (1993).
[61]A. Ichimiya, K. Kambe, and G. Lehmpfuhl, J. Phys. Soc. Jpn. **49**, 684 (1980).
[62]G. Meyer-Ehmsen, in *Reflection High Energy Electron Diffraction and Reflection Electron Imaging of Surfaces*, Vol. 188 of *NATO Advanced Study Institute, Series B: Physics*, edited by P. K. Larsen and P. J. Dobson (Plenum Press, New York, 1987), p. 99.
[63]S. L. Dudarev and M. J. Whelan, Phys. Rev. Lett. **72**, 1032 (1994).
[64]S. L. Dudarev and M. J. Whelan, Surf. Sci. **310**, 373 (1994).
[65]N. F. Mott and H. S. W. Massey, *The Theory of Atomic Collisions*, 3rd ed. (Clarendon Press, Oxford, 1965).
[66]L.-M. Peng and J. M. Cowley, Acta Crystallogr. Sect. A **42**, 545 (1986).
[67]P. Hirsch, A. Howie, R. B. Nicholson, D. W. Pashley, and M. J. Whelan, *Electron Microscopy of Thin Crystals* (Butterworth, London, 1965).
[68]*Handbook of Mathematical Functions*, edited by M. Abramowitz and I. Stegun (Dover, New York, 1963), p. 16.

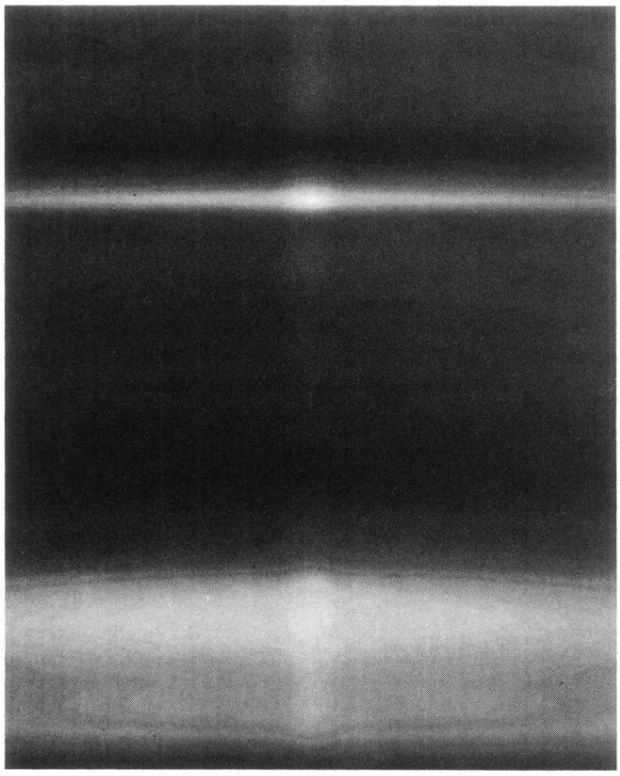

FIG. 11. The distribution of the diffuse intensity computed using the one-dimensional approximation for half a monolayer coverage ($t = 0.5\tau$) for $N^2 = 64$. A bright narrow horizontal line in the upper part of the figure is the (008) Kikuchi line, while the relatively broad enhancement of intensity at the bottom of the figure corresponds to the (004) forbidden gap in the one-dimensional band structure for the (001) row of reflections.